

Revised for ApJ February 27, 2003

## The Geometry of Resonant Signatures in Debris Disks with Planets

Marc J. Kuchner<sup>1</sup> and Matthew J. Holman

`mkuchner@cfa.harvard.edu, mholman@cfa.harvard.edu`

*Harvard-Smithsonian Center for Astrophysics, 60 Garden Street, Cambridge, MA 02138*

### ABSTRACT

Using simple geometrical arguments, we paint an overview of the variety of resonant structures a single planet with moderate eccentricity ( $e \lesssim 0.6$ ) can create in a dynamically cold, optically thin dust disk. This overview may serve as a key for interpreting images of perturbed debris disks and inferring the dynamical properties of the planets responsible for the perturbations. We compare the resonant geometries found in the solar system dust cloud with observations of dust clouds around Vega,  $\epsilon$  Eridani and Fomalhaut.

*Subject headings:* celestial mechanics — circumstellar matter — interplanetary medium — planetary systems — stars: individual ( $\alpha$  Lyrae,  $\beta$  Pictoris,  $\epsilon$  Eridani, Fomalhaut)

### 1. Introduction

Direct imaging of nearby stars can not yet detect light from extrasolar planets. However, imaging can detect circumstellar dust, and when a planet orbits inside a dust cloud, the planet can reshape the cloud dynamically, as the Earth perturbs the solar dust cloud. Several debris disks around nearby main sequence stars show structures and asymmetries which have been ascribed to planetary perturbations (Burrows et al. 1995; Holland et al. 1998; Schneider et al. 1999; Koerner et al. 2001; Holland et al. 2003); perhaps these perturbed disks are signposts of extrasolar planetary systems.

---

<sup>1</sup>Michelson Postdoctoral Fellow

Many of these disk features can be modeled as dust trapped in mean motion resonances (MMRs) with a planet. Gold (1975) suggested that as interplanetary dust spirals into the sun under the influence of Poynting-Robertson drag (P-R drag), planets could temporarily trap the dust in MMRs, creating ring-like density enhancements in the interplanetary cloud. Since then, both the InfraRed Astronomical Satellite (IRAS) and the Diffuse InfraRed Background Explorer (DIRBE) on the Cosmic Background Explorer (COBE) satellite have provided evidence for a ring of dust particles trapped by the Earth (Jackson & Zook 1989; Reach 1991; Marzari & Vanzani 1994; Dermott et al. 1994; Reach et al. 1995). Models of Kuiper Belt dust dynamics (Liou & Zook 1999) suggest that Neptune may also trap dust in first-order MMRs.

Other stars may host planets like the Earth or Neptune. However, most of the known extrasolar planets do not resemble the Earth or Neptune; they have masses in the range of 0.3–15 Jupiter masses, and they often have significant orbital eccentricities (see, e.g., the review by Marcy & Butler 2000). Simulations by Kuchner & Holman (2001) show that planets as massive as these on eccentric orbits placed in a cloud of inspiraling dust often create two concentrations of dust placed asymmetrically with respect to the star. Maps of the vicinity of Vega made with the IRAM Plateau de Bure interferometer at 1.3 mm (Wilner et al. 2002) and with the JCMT at  $850\text{ }\mu\text{m}$  (Holland et al. 1998) reveal two concentrations of circumstellar emission whose asymmetries can be naturally explained by such a model, possibly indicating the presence of a few-Jupiter mass planet in an eccentric orbit around Vega (Wilner et al. 2002). Other papers have numerically explored the interactions of particular planetary system configurations with a dust disk, with a view towards developing a general key for interpreting disk structures (Roques et al. 1994; Lecavelier Des Etangs et al. 1996; Liou & Zook 1999; Quillen & Thorndike 2002).

We assemble a primitive version of such a key by mapping the geometries of the MMRs which are likely to trap the most dust near a planet embedded in a debris disk. We illustrate the patterns formed by the libration centers of the trapped particles in an inertial frame—the frame of a distant observer. These basic patterns allow us to characterize four structures that probably span the range of high-contrast resonant structures a planet on an orbit with eccentricity up to  $\sim 0.6$  and low inclination can create in a dust disk.

Figure 1 shows these structures here for reference; we discuss them throughout the paper, particularly in Section 4. Cases I and II in this figure represent the structures formed by planets on low-eccentricity orbits. Cases III and IV represent structures created by planets on moderately eccentric orbits. Cases I and III represent structures created by planets with substantially less than 0.1% of the mass of the star; cases II and IV represent structures created by more massive planets.

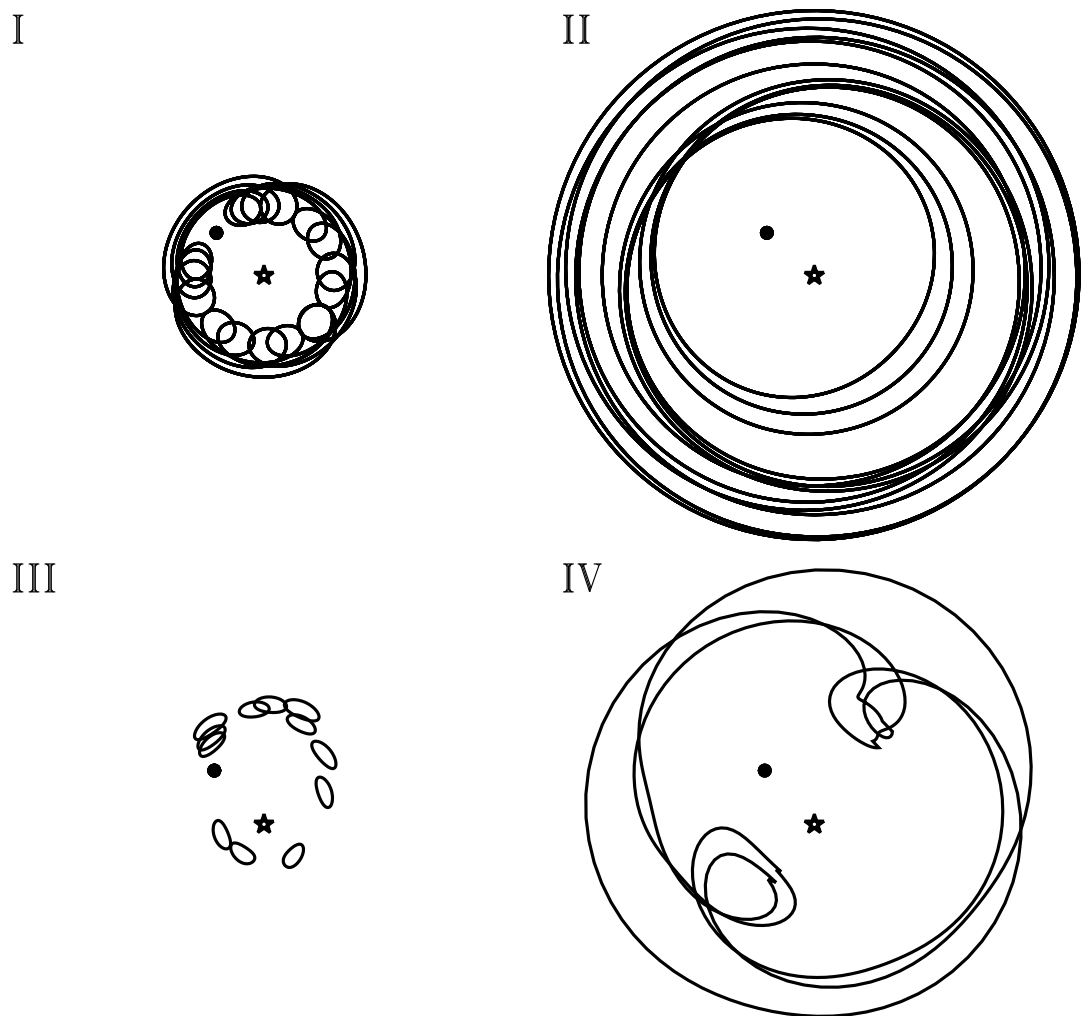


Fig. 1.— Four basic resonant structures: I) low mass planet on a low eccentricity orbit, II) high mass planet on a low eccentricity orbit, III) low mass planet, moderate eccentricity orbit, and IV) high mass planet, moderate eccentricity orbit.

## 2. PLANETS ON LOW-ECCENTRICITY ORBITS

### 2.1. Low Mass Planets

First, we review some of the physics of resonant dust rings created by relatively low mass planets, like the Earth and Neptune. In the rest of this paper, we generalize the discussion to planets with mass up to  $\sim 15$  Jupiter masses and  $e_0$  up to  $\sim 0.6$ . The resonant geometries we will describe apply to the general restricted three-body problem. However, we have in mind a source of dust, like the asteroid belt or the Kuiper belt, which releases dust on low-eccentricity orbits at semimajor axes,  $a > a_0$ , where  $a$  is the semimajor axis of the particle’s orbit and  $a_0$  is the semimajor axis of the planet’s orbit. We use the convention that quantities with a subscript 0 refer to the planet.

We do not consider interactions between the dust grains, or between dust and any gas in the disk. For example, our approach does not apply to the gaseous, optically-thick disks found around young stellar objects. However, the resonances we describe must underlie the basic resonant features of the solar system dust complex and debris disks around main sequence stars with less than a few lunar masses of dust.

The radiation forces on a particle are parametrized by  $\beta$ , the strength of the stellar radiation pressure force on a particle divided by the strength of the stellar gravitational force on a particle. For a spherical particle with radius  $s \gtrsim 1 \mu\text{m}$  and density  $2 \text{ g cm}^{-3}$  orbiting a star with mass  $M_\star$  and luminosity  $L_\star$ ,

$$\beta = \left( \frac{0.285 \mu\text{m}}{s} \right) \left( \frac{L_\star}{L_\odot} \right) \left( \frac{M_\odot}{M_\star} \right). \quad (1)$$

A typical particle in the solar system may have  $s \approx 1\text{--}100 \mu\text{m}$  (Grun et al. 1985; Fixsen & Dwek 2002), or  $\beta \approx 0.285\text{--}0.00285$ . Dust grains released at circumstellar distance  $r$  that are too large to be ejected by radiation pressure ( $\beta \lesssim 0.5$ ) spiral into the star via P-R drag (Robertson 1937; Burns et al. 1979), on a time scale

$$T_{PR} = \frac{400}{\beta} \left( \frac{M_\odot}{M_\star} \right) \left( \frac{r}{1\text{AU}} \right)^2 \text{ years.} \quad (2)$$

Other drag forces, like solar wind, may also contribute to the decay of the particle’s orbit (Banaszkiewicz et al. 1994).

Dust spiraling inwards towards a planet encounters a series of exterior MMRs, each of which is associated with terms in the disturbing function of the form

$$\langle R \rangle_{res} = \frac{Gm_0}{a} F(\alpha, e, e_0) \cos \phi, \quad (3)$$

where  $G$  is the gravitational constant,  $m_0$  is the mass of the planet, and  $\alpha = a_0/a$  (see, e.g., Brouwer & Clemence 1961; Murray & Dermott 1999). The resonant argument,  $\phi$ , is a linear combination of the orbital elements of the particle and the planet, which can be interpreted as an angle (Greenberg 1978). We do not discuss interior MMRs because they can not sustain long-term trapping (see e.g. Murray & Dermott 1999, p. 381). The potential,  $\langle R \rangle_{res}$ , causes the argument  $\phi$  to accelerate. For a particle trapped in the resonance,  $\phi$  librates about  $\phi \approx 0$  if  $F(\alpha, e, e_0) < 0$ , and  $\phi$  librates about  $\phi \approx \pi$  if  $F(\alpha, e, e_0) > 0$ . A MMR of the form  $j:k$  is nominally located at a semimajor axis given by  $1/\alpha \approx (j/k)^{2/3}(1 - \beta)^{1/3}$ .

As a particle approaches the planet from afar, it encounters stronger and stronger resonances, and has a better and better chance of becoming trapped. For particles approaching the Earth or Neptune, the first resonances which are strong enough to trap substantial amounts of dust are the first-order MMRs: resonances of the form 2:1, 3:2, 4:3, etc. To first order in eccentricity and inclination, these resonances consist of pairs of terms with arguments

$$\phi_1 = j\lambda - (j-1)\lambda_0 - \varpi \quad (4a)$$

$$\phi_2 = j\lambda - (j-1)\lambda_0 - \varpi_0, \quad (4b)$$

where  $\lambda$  and  $\lambda_0$  are the mean longitudes of the particle and the planet, and  $\varpi$  and  $\varpi_0$  are the longitudes of pericenter of the particle and the planet, respectively. For the Earth ( $e_0 = 0.017$ ) and Neptune ( $e_0 = 0.0086$ ), the  $\phi_1$  resonance dominates at all values of  $\varpi$  if the dust particle has even a small orbital eccentricity, and  $\phi_1$  librates about  $\phi_1 \approx \pi$ . Passage through this resonance slowly raises the particle's eccentricity, which asymptotically approaches a limiting value,  $e_{max}$ , when the dynamics are followed using an expansion to second order in  $e$  (Weidenschilling & Jackson 1993; Sicardy et al. 1993; Beauge & Ferraz-Mello 1994; Liou & Zook 1997):

$$e_{max} = \sqrt{2/(5j)}. \quad (5)$$

In the process, the particle's orbit becomes planet crossing, and in a matter of a few P-R times, the particle generally leaves the resonance via a close encounter with the planet (Marzari & Vanzani 1994) and an abrupt transition to a new orbit with a different eccentricity and semimajor axis. Near the Earth, trapped dust populates several first-order MMRs.

The condition that  $\phi_1$  librates about  $\phi_1 \approx \pi$  provides a relationship between  $\lambda$  and  $\varpi$ . Since rotations of the whole system by  $2\pi$  must not affect the dynamics, we can write that the libration centers are located where

$$\lambda \approx ((j-1)(\lambda_0 + 2\pi K) + \varpi + \pi)/j \quad \text{for } K \in \mathcal{Z}. \quad (6)$$

Figure 2 shows how this condition leads to the formation of a density wave, using the 3:2 MMR as an example. Figure 2a shows a variety of elliptical dust orbits, all with the same

$1/\alpha = 1.31$  and  $e = 0.8e_{max}$ , but with different  $\varpi$ 's. According to Equation 6, each one of these orbits has  $j = 3$  different longitudes that may be libration centers for a particle trapped in the  $\phi_1$  term. Figure 2b shows these three locations, marked with X's, for each of two elliptical orbits with slightly different  $\varpi$ 's.

Figure 2c shows the locus of the libration centers for the whole range of elliptical orbits shown in Figure 2a. In Figure 2d, the planet has moved to a new longitude, and following Equation 6, so have the libration centers. The density wave formed by the trapped particles resembles the pattern formed by the libration centers, blurred somewhat by libration, mostly in the azimuthal direction. Ozernoy et al. (2000) shows some examples of how libration blurs the patterns formed by particles trapped in individual resonances.

Though any individual particle in Figure 2 moves steadily counterclockwise, slower than the planet, the density wave appears to rotate as a fixed pattern together with the planet. At conjunction ( $\lambda = \lambda_0$ ) the resonance condition implies that  $\varpi \approx \lambda_0 + \pi$ , so the libration centers just outside the planet are always near apocenter. This condition creates the signature gap at the location of the planet seen in simulations of the Earth's ring (Dermott et al. 1994) and of Kuiper Belt dust interacting with Neptune (Liou & Zook 1999) and illustrated in Figure 1 (Case I).

## 2.2. Higher Mass Planets

We can understand the range of possible resonant dust cloud structures by understanding the density-wave patterns created by the series of MMRs that are likely to trap dust near a planet. Table 1 lists the arguments in a series of MMRs that figure most prominently in the sculpting of dust clouds (ignoring the planet's inclination, which first appears with order inclination squared) in order by  $\alpha$ . It also lists the corresponding leading terms in  $F(\alpha, e, e_0)$ , evaluated for  $\mu = 1/1047$  (i.e. Jupiter), and  $\beta \ll 1$ . The first MMRs in the list are the first-order resonances described above.

For a given planet/dust cloud combination, a few MMRs generally dominate the observed resonant structure. In simulations of  $\beta = 0.037$  dust particles approaching the Earth (Dermott et al. 1994), the first-order  $j = 4$ –10 MMRs dominate the appearance of the trapped dust cloud. In simulations of Neptune's ring by Liou & Zook (1999), the 2 : 1 and 3 : 2 resonances ( $j = 2$  and  $j = 3$ ) dominate the appearance of the dust cloud.

The factor of  $Gm_0/a$  in Equation 3 makes MMRs at large  $a$  weaker and less able to trap substantial quantities of dust. But for more massive planets, the trapping probability for all MMRs is higher (Lazzaro et al. 1994), so particles approaching from afar become trapped

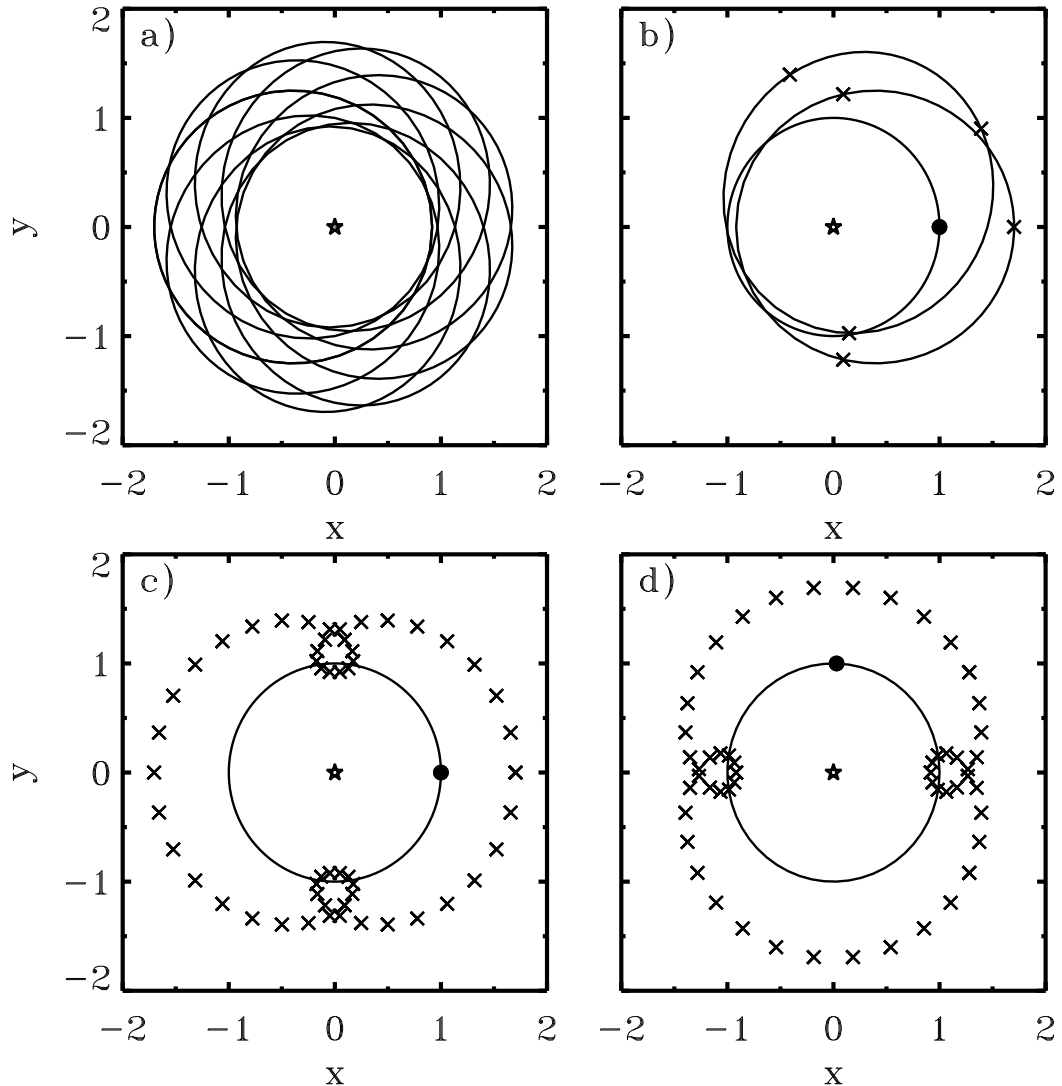


Fig. 2.— How a planet on a low eccentricity orbit creates density waves. a) Several particle orbits with different  $\varpi$ 's. b) Libration centers of the  $3\lambda - 2\lambda_0 - \varpi$  term on two of these orbits, indicated by X's. c) The locus of all the libration centers. d) The density wave appears to orbit at the same angular frequency as the planet (located at the filled circle).

sooner, in MMRs with longer orbital periods and larger semimajor axes. Likewise, close encounters with the planet more easily scatter dust grains out of exterior MMRs at small  $a$ , and this effect worsens with the mass of the planet.

The MMRs near the planet also become close together and begin to compete with one another. If  $\mu = m_0/M_*$ , the resonance overlap criterion (Wisdom 1980; Duncan et al. 1989) predicts that first-order resonances with  $j > 0.45(\mu(1 - \beta))^{-2/7} + 1$  are completely chaotic. This condition appears to place an absolute limit on how far down the chain of resonances a dust particle can be trapped. For large particles near the Earth ( $\mu \approx 3 \times 10^{-6}$ ), this criterion predicts that the first completely overlapped MMR is 17:18, for Neptune ( $\mu \approx 5 \times 10^{-5}$ ), it is 8:9, and for Jupiter ( $\mu \approx 10^{-3}$ ) it is 4:5.

As we have mentioned, many of the observed extrasolar planets have substantially more mass than planets in the solar system. Such massive planets quickly scatter dust from their first-order MMRs. So after the first-order resonances, Table 1 lists the  $n:1$  resonances, the lowest order terms available at large semimajor axes—beyond the 2:1 MMR (nominally located at  $a/a_0 = 1.59$ ). In numerical integrations, Kuchner & Holman (2001) and Wilner et al. (2002) found that dust spiraling inwards towards a massive planet became trapped in this series of  $n:1$  resonances. Table 1 shows that the terms in these resonances which don't depend on the eccentricity of the planet have the form  $j\lambda - \lambda_0 - (j - 1)\varpi$ . These terms must dominate when  $e_0$  is small.

The  $j\lambda - \lambda_0 - (j - 1)\varpi$  terms in Table 1 are mostly positive, so most of these arguments librate around  $\pi$ . However these terms all include contributions from indirect terms, which arise from the reflex motion of the star. The indirect contributions tend to reduce the strength of the resonance, and in the case of the 3:1, this effect makes the coefficient negative, so the  $3\lambda - \lambda_0 - 2\varpi$  argument librates around 0.

The libration centers for the terms which librate around  $\pi$  are located at

$$\lambda \approx ((j - 1)\varpi + \lambda_0 + \pi(1 + 2K))/j, \quad \text{for } K \in \mathcal{Z}. \quad (7)$$

Again there are  $j$  libration centers spaced evenly around each elliptical dust orbit, and again, the locus of libration centers appears to co-rotate with the planet. But this time, when we set  $\lambda = \lambda_0$ , we find that at conjunction, the particle can be in one of a few different places;

$$\varpi \approx \lambda_0 - \pi(1 + 2K)/(j - 1) \quad \text{at conjunction.} \quad (8)$$

One can also show following Weidenschilling & Jackson (1993), for example, that passage through a pure  $j\lambda - \lambda_0 - (j - 1)\varpi$  term raises the eccentricity of a dust particle in the same way that passage through a  $j\lambda - (j - 1)\lambda_0 - \varpi$  term does, and that the limiting eccentricity

is again given by Equation 5. We can generate a rough picture of the density waves created by the dust trapped in these terms in the same manner as Figure 2, by drawing a variety of elliptical orbits with eccentricity  $e \approx e_{max}$  at an appropriate semimajor axis, and using Equation 7 (and Kepler’s equation) to locate the libration centers on these orbits.

Figure 3 shows the patterns created by the most important resonant terms listed in Table 1. The first column of Figure 3 shows patterns for the terms which appear when the planet’s eccentricity is low: the  $j\lambda - (j-1)\lambda_0 - \varpi$  terms for first-order resonances, and the  $j\lambda - \lambda_0 - (j-1)\varpi$  terms for  $n:1$  resonances. The patterns are the locii of the libration centers, generated in the manner of Figure 2.

### 3. PLANETS ON ECCENTRIC ORBITS

The patterns in the first column of Figure 3 appear in the textbook by Murray and Dermott (1999, p. 325), derived in a slightly different context—by tracing the path of a particle in a frame corotating with the planet. However, the literature offers little discussion of resonant structures created by planets on eccentric orbits, and this case is crucial for understanding extrasolar planetary systems. Naturally, for a planet on an eccentric orbit, there is no simple corotating frame. But we can deduce the resonance patterns associated with planets on eccentric orbits by building on the arguments used above.

#### 3.1. Secular Effects

Besides resonant perturbations, planets introduce secular perturbations to the orbits of nearby particles. When the planet’s orbit is eccentric, these perturbations generally produce a correlation between  $e$  and  $\varpi$ . We must consider these effects when we examine MMRs with planets on eccentric orbits.

We can demonstrate the importance of secular perturbations by comparing them with radiation forces. Near a planet, the P-R time, and thereby the trapping time, is longer than the secular time scale for dust grains with  $\beta < \beta_0$ , where

$$\beta_0 = 100 \left( \frac{M_*}{M_\odot} \right)^{-1/2} \left( \frac{a}{1 \text{AU}} \right)^{1/2} \alpha b_{3/2}^1(\alpha) \mu, \quad (9)$$

and the Laplace coefficient (size  $\sim$  unity) is

$$b_{3/2}^m(\alpha) = \frac{1}{\pi} \int_0^{2\pi} \frac{\cos m\psi \, d\psi}{(1 - 2\alpha \cos \psi + \alpha^2)^{3/2}}. \quad (10)$$

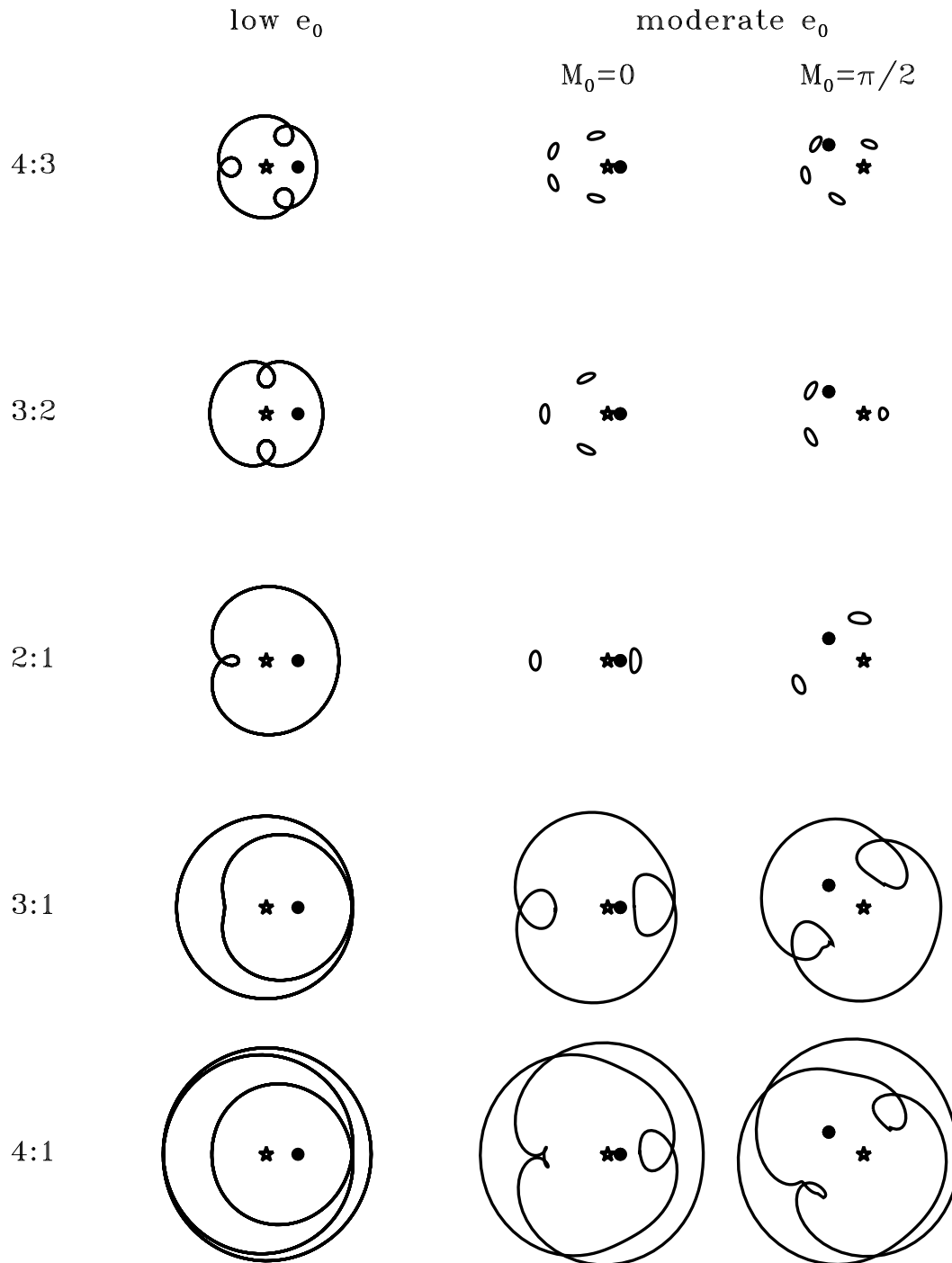


Fig. 3.— Patterns formed by dust in MMRs listed in Table 1.

I.e.,  $\beta_0 \sim 100\mu$ . For example,  $\beta_0 = 0.022$  for Neptune,  $\beta_0 = 0.44$  for a Jupiter-mass planet orbiting Vega at  $a = 40$  AU. So we can expect most observable particles in the cases we are interested in ( $10^{-5} \lesssim \mu \lesssim 10^{-2}$ ) to suffer significant secular evolution while they are trapped in a MMR. Secular perturbations from planets with eccentric orbits affect all dust particles in their vicinity, even those which are not in strong MMRs.

In the Laplace-Lagrange description of secular perturbations, valid for  $e, e_0 \ll 1$ , a particle's osculating  $e$  and  $\varpi$  are expressed as a combination of a constant forced elements,  $e_{forced}$  and  $\varpi_{forced}$ , and time-varying free elements,  $e_{free}$  and  $\varpi_{free}$ . Secular evolution is easily visualized in the  $(h, k)$  coordinate system, where  $h = e \cos \varpi$  and  $k = e \sin \varpi$ . In this system, we write  $h = h_{forced} + h_{free}$ , and  $k = k_{forced} + k_{free}$ .

When there is only a single perturbing planet on a fixed orbit, the particle's forced elements are constant, and the osculating elements,  $h$  and  $k$ , trace out a circle centered on  $(h_{forced}, k_{forced})$  with a radius of  $e_{free}$ . The forced longitude of pericenter is  $\varpi_{forced} = \arctan(k_{forced}/h_{forced}) = \varpi_0$ , and the forced eccentricity is

$$e_{forced} = \sqrt{h_{forced}^2 + k_{forced}^2} = \frac{b_{3/2}^2(\alpha)}{b_{3/2}^1(\alpha)} e_0. \quad (11)$$

As  $a$  approaches  $a_0$ ,  $e_{forced}$  approaches  $e_0$ . Table 1 lists the approximate value of  $e_{forced}/e_0$  at the nominal  $\alpha$  for each MMR.

In a cloud of many particles, many orbits with a range of  $h_{free}$  and  $k_{free}$  are occupied. However, all particles with a given semimajor axis will have the same  $h_{forced}$  and  $k_{forced}$ . For example, if all particles are released on circular orbits outside the planet's orbit and outside of any MMRs, then the Laplace-Lagrange solution prescribes that at any given time all the particles with a given semimajor axis will occupy a circle with radius  $e_{free}$  centered on the point  $(h_{forced}, k_{forced})$  in the  $(h, k)$  plane. Dermott et al. (1985) and Wyatt et al. (1999) showed that a set of orbits occupying such a circle in the  $(h, k)$  plane form a cloud that is roughly circular, but the center of the cloud is offset from the star a distance  $e_0 a_0$  along the planet's apsidal line in the direction of the center of the planet's orbit. Hence, the background dust cloud in the vicinity of a large planet should often appear circular in the absence of MMRs, though if the planet's orbit is eccentric, the center of the circle will be offset from the star.

When the perturber has higher eccentricity, or when a particle is in a MMR, the particle's secular trajectory changes somewhat; the orbit no longer traces an exact circle in the  $(h, k)$  plane, even when the librations are averaged away (Wisdom 1983). However, the character of the averaged secular motion often remains the same;  $h$  and  $k$  follow a simple closed loop around  $(h_{forced}, k_{forced})$ . We will retain the spirit of the Laplace-Lagrange approximation for

the secular motion of the particles for the remainder of this paper, and we will refer loosely to free and forced elements, even when we are discussing resonant orbits. We find that this approximation suffices for our broad exploration of planetary signatures in debris disks.

### 3.2. Mean Motion Resonances

When a particle is trapped in a MMR with a planet on a circular orbit, the resonant argument which only depends on  $\varpi$ , not on  $\varpi_0$  dominates the particle's motion. The other terms in the resonance have coefficients  $F(e, e_0)$  that are zero when  $e_0$  is zero. However, when a particle is trapped in a MMR with a planet on an eccentric orbit, resonant arguments which depend on  $\varpi_0$  may come into play.

To leading order, the averaged disturbing function for a MMR with a planet on an eccentric orbit is the sum of two or more terms:

$$\langle R \rangle_{res} = \frac{Gm_0}{a} \sum_{\xi} F_{\xi}(\alpha, e, e_0) \cos \phi_{\xi}, \quad (12)$$

where, as Table 1 shows,  $\phi_1 = p\lambda - q\lambda_0 + (p - q)\varpi$  and  $\phi_{\xi} = \phi_1 + (\xi - 1)(\varpi - \varpi_0)$ . Following Wisdom (1983), we can re-express this sum as

$$\langle R \rangle_{res} = \frac{Gm_0}{a} F'(\alpha, e, e_0, \varpi, \varpi_0) \cos \phi', \quad (13)$$

where

$$\phi' = \phi_1 + \arctan \left( \frac{\sum_{\xi=2}^p |F_{\xi}| \sin ((\xi - 1)(\varpi - \varpi_0) + \delta_{\xi})}{|F_1| + \sum_{\xi=2}^p |F_{\xi}| \cos ((\xi - 1)(\varpi - \varpi_0) + \delta_{\xi})} \right) \quad (14)$$

and

$$F'(\alpha, e, e_0, \varpi, \varpi_0) = \sqrt{\left( \sum_{\xi} F_{\xi}(\alpha, e, e_0) \sin \phi_{\xi} \right)^2 + \left( \sum_{\xi} F_{\xi}(\alpha, e, e_0) \cos \phi_{\xi} \right)^2}. \quad (15)$$

The quantity  $\delta_{\xi} = \pi$  for  $F_{\xi} < 0$ , and  $\delta_{\xi} = 0$  otherwise. We define  $F'$  to be always  $\geq 0$ , so on resonance, the new argument,  $\phi'$ , librates around  $\phi' \approx \pi$ . Equation 14 shows explicitly that the differences among the terms only appear on a secular time scale, as  $\varpi - \varpi_0$  precesses.

At any moment, the particle's orbit may be viewed as undergoing libration about  $\phi' = \pi$ . This change in the effective resonant argument can change the constraints on the orbital elements of resonant objects, which can result in dramatically different-looking clouds of trapped particles. Often one term dominates, in the sense that  $\phi' \approx \phi_{\xi}$  or  $\phi' \approx \phi_{\xi} + \pi$ . This

circumstance depends on  $e$ ,  $e_0$ ,  $\varpi$ , and  $\varpi_0$ , and the details of trapping, but we can appeal to numerical simulations and use what we know about the secular evolution of dust particles to help decide which terms are likely to be most important.

### 3.3. High Mass Planets

It is easier to consider high mass planets first, because the  $n:1$  resonances that dominate the appearance of dust clouds containing a massive planet are farther from the planet than the first-order resonances which dominate in the case of a low mass planet. Particles released on circular orbits approach a planet with  $e_{\text{free}} \approx e_{\text{forced}}$ , so they reach the  $n:1$  MMRs with  $e$  ranging from 0 to  $e_{\text{forced}} + e_{\text{free}}$ . As Table 1 shows,  $e_{\text{forced}} \approx e_0/2$  near the lowest order  $n:1$  MMRs. When  $\varpi \approx \varpi_0 + \pi$ , all the terms become degenerate, in the sense that all of their libration centers occur at the same longitudes. At the other end of the range of secular motion,  $\varpi \approx \varpi_0$ , and  $e \approx e_0$ , so according to Equation 14, the term with the largest coefficient in  $F(\alpha, e, e_0)$  will dominate the motion of the particles.

The arguments which match the terms with the largest coefficients in  $F(\alpha, e, e_0)$  (see Table 1) share a second common form:  $j\lambda - \lambda_0 - \varpi_0 - (j - 2)\varpi$ . Numerical integrations (Wilner et al. 2002) confirm that these terms to dominate the resonant dynamics over a wide range of planet eccentricities. These terms always have  $F(\alpha, e, e_0) < 0$ , so the corresponding arguments librate about 0. The  $j$  libration centers on each ellipse are located at

$$\lambda \approx (\lambda_0 + \varpi_0 + (j - 2)\varpi + 2\pi K)/j, \quad \text{for } K \in \mathcal{Z}. \quad (16)$$

We reserve a discussion of the complicated secular dynamics of these resonances for a future paper.

Figure 4 illustrates the pattern formed by particles in the  $3\lambda - \lambda_0 - \varpi_0 - \varpi$  term near a planet with  $e_0 = 0.6$ . Once a particle is trapped in resonance, its secular evolution no longer obeys the Laplace-Lagrange solution, but the libration centers of the trapped particles will still occupy a closed curve in the  $(h, k)$  plane. Figure 4a shows such a variety of orbits centered on  $h = 0.58e_0$ ,  $k = 0$ . Orbits which are close to apse-alignment with the planet have higher eccentricities. Like the Laplace-Lagrange orbit distributions discussed by Dermott et al. (1985) and Wyatt et al. (1999), these orbits taken together form a pattern which is roughly circular, but the center of the circle is offset from the star along the planet's apsidal line in the direction of the center of the planet's orbit.

Figure 4b shows the 3 libration centers on two of these orbits, calculated from Equation 16. By definition,  $\lambda = M + \varpi$ , where  $M$  is the particle's mean anomaly. For particles

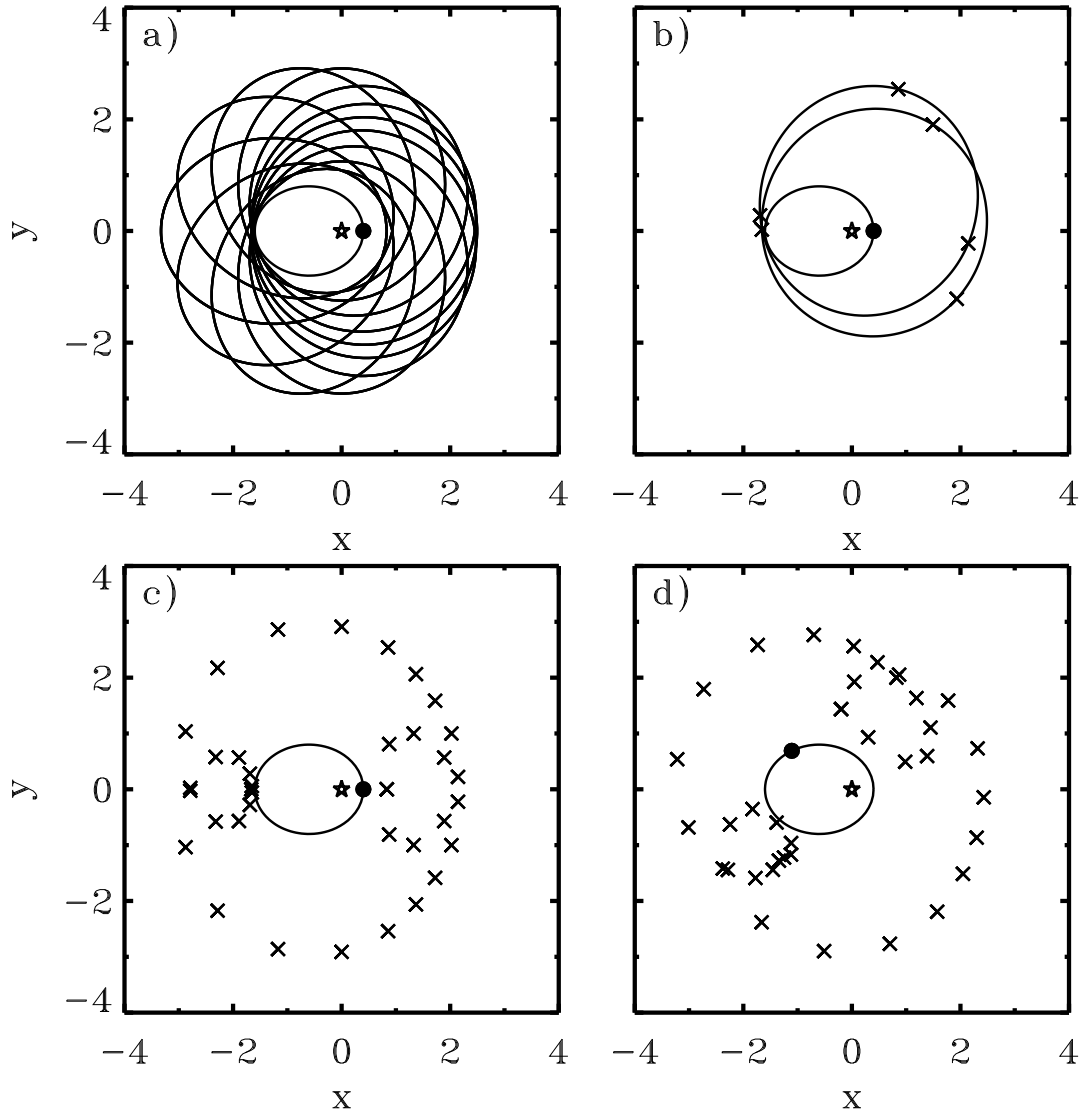


Fig. 4.— Libration centers of the  $3\lambda - \lambda_0 - \omega_0 - \omega$  term. a) Several particle orbits with different  $e$  and  $\omega$ . b) The libration centers on two of these orbits when the planet is at pericenter. c) All the libration centers. d) The clumps formed by particles trapped in this term appear to rotate at half the angular frequency of the planet.

at pericenter,  $M = 0$  and  $\lambda = \varpi$ , so for particles trapped in *any*  $j\lambda - \lambda_0 - \varpi_0 - (j - 2)\varpi$  term,

$$\varpi \approx M_0/2 + \varpi_0 + \pi K \quad \text{for } K \in \mathcal{Z}, \quad (17)$$

where  $M_0$  is the planet's mean anomaly. In other words, the libration centers for this family of terms reach pericenter at two different longitudes, and these special longitudes precess at an angular frequency equal to half the Keplerian angular frequency of the planet. When the planet reaches pericenter ( $M_0 = 0$ ), so do the particles on orbits that are apse-aligned or anti-apse-aligned with the planet's orbit. Figures 4c and d show that the locus of libration centers makes a characteristic two-lobed pattern, which appears to rotate at half the mean angular frequency of the planet. The center of this apparent rotation lies on the planet's apsidal line between the star and the center of the planet's orbit.

### 3.4. Low Mass Planets

The resonances populated near low-mass planets cluster at semimajor axes near the planet's semimajor axis, where  $e_{forced} \approx e_0$ . In this vicinity, the resonant orbits can easily become planet-crossing unless they are roughly apse-aligned with the planet's orbit, i.e.  $e_{free} < e_{forced}$ , and  $\varpi \approx \varpi_0$ . Figure 5a shows a collection of roughly apse-aligned orbits, all with  $e_{forced} = 0.5$ , and  $e_{free} = 0.12$ . In the absence of MMR's, the combination of these elliptical orbits would appear as an elliptical ring.

For the case of the 3:2 MMR, a single one of these orbits has three libration centers, shown in Figure 5b. For a family of orbits that must remain roughly apse-aligned with the planet, the secular spread in the libration centers is necessarily small, and the resonant arguments are all roughly equal. So, as Figure 5c shows, we should expect the density wave to resemble the pattern produced by the libration centers in any one orbit; the libration centers associated with any MMR of the form  $j:k$  form a set of  $j$  clumps. As Figure 5d shows, the locus of all the libration centers orbits at  $k/j$  times the angular frequency of the planet; when the planet's mean anomaly changes by  $\pi/2$ , the mean anomalies of the clumps of particles in the 3:2 MMR change by  $\pi/3$ .

An exterior first-order MMR has two relevant terms (Equations 4a and 4b), and for the second term,  $F_2(\alpha, e, e_0) < 0$ . For this case, Equation 15 becomes

$$\phi' = \phi_1 + \arctan \left( \frac{|F_2(\alpha, e, e_0)| \sin(\varpi - \varpi_0 + \pi)}{|F_1(\alpha, e, e_0)| + |F_2(\alpha, e, e_0)| \cos(\varpi - \varpi_0 + \pi)} \right). \quad (18)$$

A key difference between the two terms is that one argument librates around 0, the other around  $\pi$ .

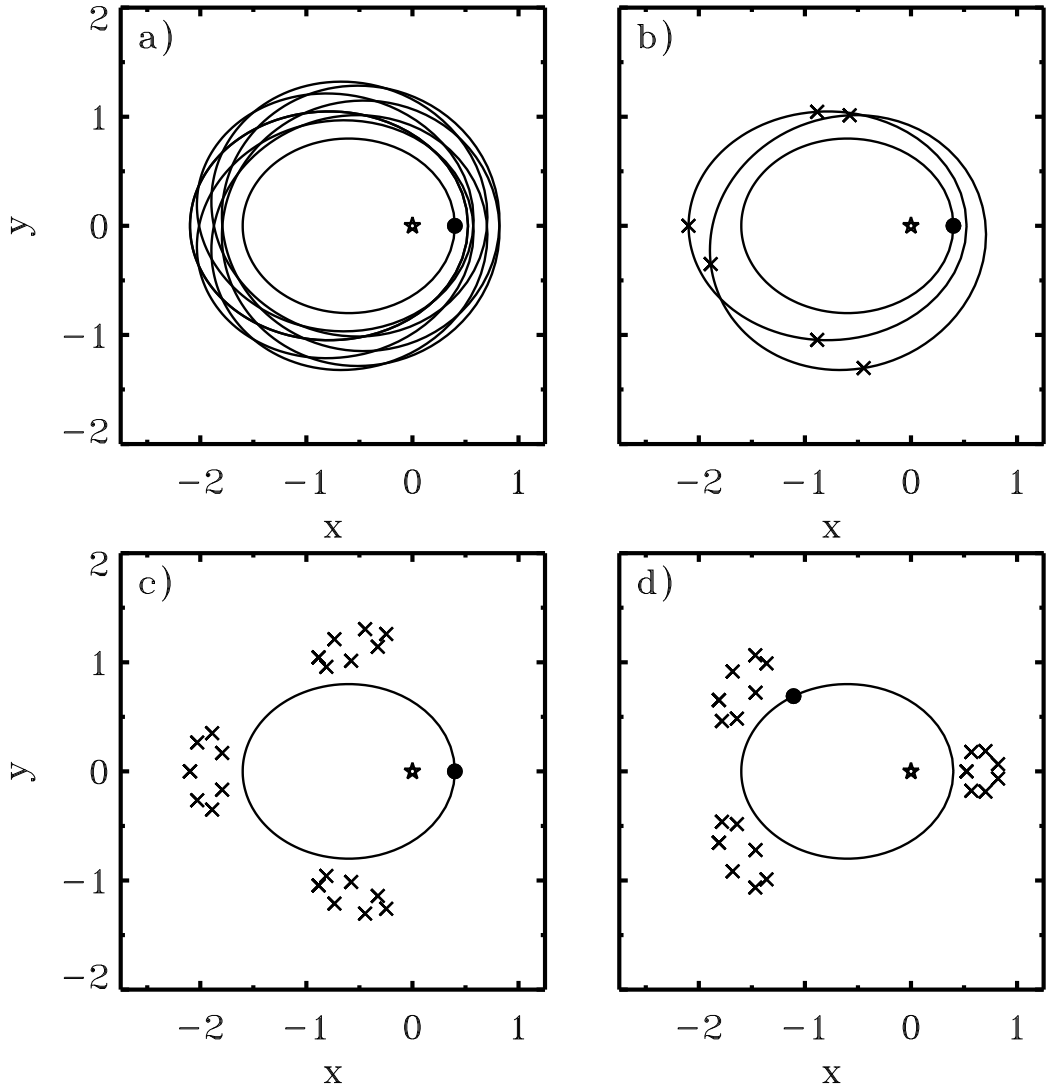


Fig. 5.— How dust confined to the 3:2 MMR near a planet on a moderately eccentric orbit might appear. a) Several orbits with different  $e$  and  $\varpi$ , distributed in a Laplace-Lagrange circle with small  $e_{free}$ . b) The libration centers on two of these orbits when the planet is at pericenter. c) All the libration centers. d) The three dust clumps really do orbit at 2/3 of the planet's orbital frequency.

Deciding which resonances dominate in the vicinity of a low mass planet on an eccentric orbit can be tricky. When  $|F_1(\alpha, e, e_0)| \gg |F_2(\alpha, e, e_0)|$ ,  $\phi' \approx \phi_1$ . When  $|F_1(\alpha, e, e_0)| \ll |F_2(\alpha, e, e_0)|$ ,  $\phi' \approx \phi_2 + \pi$ . However, when  $F_1(\alpha, e, e_0) \approx F_2(\alpha, e, e_0)$ , the two terms tend to cancel each other, that is,  $|F'| \approx |F_1 - F_2|$  when  $\varpi \approx \varpi_0$ . This cancellation diminishes the strength of the resonance.

So we should expect first-order resonances to be relatively weak for a dust particle whose orbit has been secularly apse-aligned with the planet’s orbit. At  $e = e_{forced}$ , the  $\phi_1$  resonance generally has the larger coefficient. The 2:1 MMR is an exception, because  $F_1$  for the 2:1 is diminished by an indirect term, so the  $\phi_2$  resonance easily dominates. We leave it to numerical studies (Quillen & Thorndike 2002) to decide which MMRs and terms dominate in a given system containing a low mass-high eccentricity planet. However, no matter which MMRs dominate, we expect the same generic behavior; the trapped dust will form an eccentric ring of dust clumps.

## 4. PLANETARY SIGNATURES

### 4.1. Four Basic Cloud Structures

The first column of Figure 3 illustrates the density waves formed by the resonant terms we expect will dominate the appearance of dust clouds near planets with low orbital eccentricity. The second and third columns illustrate the density waves formed by the resonant terms we expect will dominate near planets with moderate orbital eccentricity: the  $j\lambda - (j-1)\lambda_0 - \varpi_0$  terms for first-order resonances, and the  $j\lambda - \lambda_0 - \varpi_0 - (j-2)\varpi$  terms for  $n:1$  resonances. In the second column, the planet is at pericenter; in the third column, the planet is at  $M_0 = \pi/2$ .

Our map of these basic patterns prepares us to consider more generally the appearance of a dust disk in the vicinity of a planet, where trapped dust occupies several MMRs. Now we can describe the origin of the structures shown in Figure 1; they are superpositions of the patterns shown in Figure 3.

Cases I and II are superpositions of the patterns depicted in the left-hand column of Figure 3. Cases III and IV are superpositions of the patterns depicted in the right-hand column of Figure 3 (and also in the middle column, at a different planetary orbital phase). In general, the rings created by the low-eccentricity planets appear to co-rotate with the planet, but the resonant structures created by moderate-eccentricity planets do not, because the density wave patterns associated with the resonances they excite vary with the planet’s orbital phase.

**Case I:** A low mass planet with low orbital eccentricity, like the Earth or Neptune, traps dust in first-order  $j\lambda - (j-1)\lambda_0 - \varpi$  resonances. Case I in shows a superposition of patterns produced by terms of this form, the patterns in the upper left-hand column of Figure 3. Populating these resonances creates a ring with a gap at the location of the planet.

**Case II:** A higher mass planet on a low-eccentricity orbit traps dust in more distant  $n:1$  resonances, in terms of the form  $j\lambda - \lambda_0 - (j-1)\varpi$ . Case II shows superpositions of patterns produced by such terms, the patterns in the lower left-hand column of Figure 3. These resonances create a larger ring with a smooth central hole.

**Case III:** A low mass planet on a moderately eccentric orbit traps dust in MMRs with small secular motion near apse-alignment with the planet, creating a blobby eccentric ring. The blobs in this ring appear to be continually created and destroyed, as dust clumps occupying different MMRs pass through one another. The more highly concentrated clumps are located near the apocenter of the planet’s orbit, where all the particles in the  $j\lambda - (j-1)\lambda_0 - \varpi_0$  terms (except for the 2:1) are constrained to have their conjunctions. The planet may or may not be located near a gap in the ring.

**Case IV:** A high mass planet on a moderately eccentric orbit creates a ring offset from the star containing a pair of clumps, where the two-lobed patterns of all the  $n:1$  resonances of the form  $j\lambda - \lambda_0 - (j-2)\varpi - \varpi_0$  coincide. The clumps appear to orbit a point along the planet’s apsidal line, between the star and the planet, at half the mean orbital frequency of the planet.

Naturally, intermediate cases will result in more than one variety of resonance being populated by dust particles; these clouds can possess features of more than one of the extreme cases shown in Figure 1. For example, an intermediate mass planet on a low eccentricity orbit will have a slightly larger ring with a less prominent gap at the location of the planet than Case I. A planet with intermediate eccentricity may have both a ring component and blobs, though librational motion may smear these blobs so that they blend into the ring.

#### 4.2. Strong Drag Forces; Wakes

When the drag force is large and the planet’s mass is small, the libration centers can shift substantially from  $\pi$ . For a MMR containing a collection of resonant arguments of the form  $\phi = j\lambda - k\lambda_0 - (j-1)\varpi - (\xi-1)(\varpi_0 - \varpi)$ , the resonant perturbations are

$$\left[ \frac{da}{dt} \right]_{Res} = -2jan\mu F'(\alpha, e, e_0, \varpi, \varpi_0) \sin \phi' \quad (19)$$

$$\left[ \frac{de}{dt} \right]_{Res} = -n\mu F'(\alpha, e, e_0, \varpi, \varpi_0) \sin \phi', \quad (20)$$

where the particle's angular frequency,  $n$ , on resonance is nominally

$$n = (GM_\star(1 - \beta)/a^3)^{1/2}. \quad (21)$$

PR drag causes relatively slow changes in  $a$  and  $e$  (Wyatt & Whipple 1950):

$$\left[ \frac{da}{dt} \right]_{PR} = \frac{-GM_\star\beta}{ac} \frac{(2 + 3e^2)}{(1 - e^2)^{3/2}} \quad (22)$$

$$\left[ \frac{de}{dt} \right]_{PR} = \frac{-5GM_\star\beta}{2a^2c} \frac{(2 + 3e^2)}{(1 - e^2)^{1/2}} \quad (23)$$

where  $c$  is the speed of light. To locate the libration centers, we set  $[da/dt]_{PR} + [de/dt]_{PR} = 0$ , and find

$$\sin \phi_0 = -\frac{(GM_\star/a)^{1/2}\beta(1 - \beta)}{2j\mu c F'(\alpha, e, e_0, \varpi, \varpi_0)} \frac{(2 + 3e^2)}{(1 - e^2)^{3/2}}. \quad (24)$$

On resonance,  $\phi'$  librates around  $\phi_0$ , which is greater than  $\pi$ .

For the case of a planet on a circular orbit, the observable effect on a dust cloud is a shift in the locations of the pericenters of the orbits of the trapped particles. In the absence of this effect, the libration centers first reach pericenter an angle  $\pi/k$  behind the planet. With this effect, the first pericenter is located closer to the planet, at an angle  $(2\pi - \phi_0)/k$ . This asymmetry concentrates the trapped dust from the Earth's ring into a blob trailing the Earth, sometimes called the Earth's "wake" (Dermott et al. 1994; Reach et al. 1995).

Figure 6 shows an example of how cases I and III, as illustrated in Figure 1, could appear when the perturber's gravity is weak compared to the drag force and the shifts in the libration centers are substantial. Case I shows a wake trailing the planet. For the terms illustrated in columns two and three of Figure 3, the shift in the libration center appears as a displacement of the density enhancements. The  $n:1$  resonance clumps will appear at  $\varpi = K\pi + M_0/2 + \varpi_0 + (\phi_0 - \pi)/2$ , i.e. their longitudes shift by  $(\phi_0 - \pi)/2$ . The first-order resonance clumps near low-mass planets on moderately eccentric orbits (Case III) shift by  $(\phi_0 - \pi)/k$  in the prograde direction.

This effect depends on the velocity of the dust ( $\sim (GM_\star/a)^{1/2}$ ), on  $\beta$ , and on the mass of the planet; it is more pronounced for small dust grains and low-mass planets close to massive and luminous stars. It is negligible for patterns generated by more massive planets (cases II and IV), even if the planets are in 3-day orbits. Moreover, this effect does not appear in simulations of Neptune's ring (Liou & Zook 1999) since even Neptune has high mass (and low orbital velocity) compared to the Earth. The  $\epsilon$  Eridani ring seen by the JCMT (Holland et al. 1998) probably does not show this effect either for the same reasons.

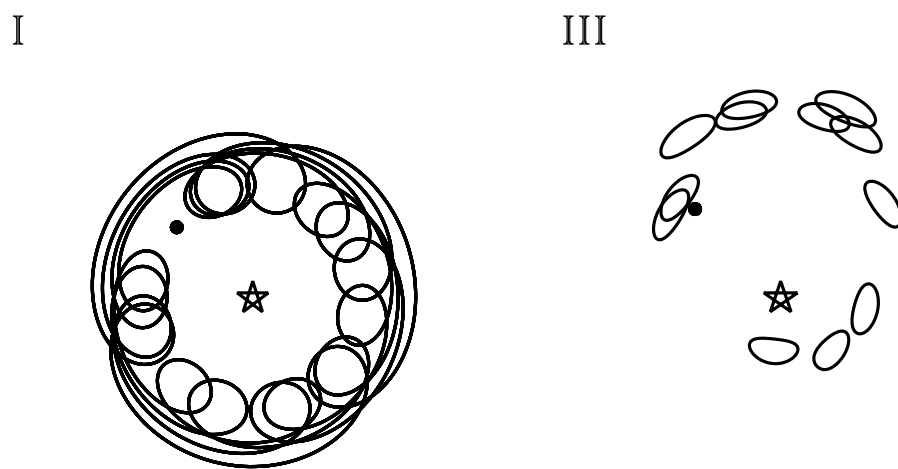


Fig. 6.— Cases I and III when the drag force is particularly strong and the planet's mass is small. Case I develops a “wake” trailing the planet. The blobs in Case III shift in the prograde direction.

## 5. DISCUSSION

### 5.1. Observed Examples

Earth is the only planet in the solar system whose resonant ring has been detected (Kuchner et al. 2000). This wake in this ring produces an asymmetry in the thermal infrared background between the direction leading the Earth and the direction trailing the Earth, which IRAS and COBE DIRBE detected (Reach 1991; Dermott et al. 1994; Reach et al. 1995). Indeed, the Earth’s ring is the only observed resonant dust cloud structure—in the solar system or elsewhere—identified with an independently observed planet! However, models of Kuiper belt dust interacting with the outer planets suggest that Neptune also creates a type I ring with a characteristic hole at the location of the planet.

Images of nearby stars with debris disks supply further examples of rings which point to undetected planets. Dust clouds around Vega,  $\beta$  Pictoris,  $\epsilon$  Eridani and Fomalhaut have all been imaged at submillimeter wavelengths (Holland et al. 1998; Greaves et al. 1998; Holland et al. 2003). The  $\beta$  Pictoris disk is edge-on, making its resonant rings hard to distinguish—if it has any. However, the other systems appear to contain resonant rings which may be easier to classify.

**Vega:** The Vega debris disk may provide an example of case IV. Submillimeter images of Vega (Wilner et al. 2002) show two concentrations of emission that resemble those in Figure 1; they are not co-linear with the star, and one is closer to the star than the other. Wilner et al. (2002) used this model to estimate that the perturbing planet has mass  $\mu \approx 10^{-3}$  and eccentricity  $e \approx 0.6$ , and used the locations of the two knots of emission to infer the planet’s current location.

**$\epsilon$  Eridani:** Case III may be a good model for the  $\epsilon$  Eridani dust ring, which has roughly four major concentrations of emission irregularly placed around the ring, and an apparent gap in the ring. As Figure 1 shows, the low-mass, moderate eccentricity planet model naturally explains the presence of a few dust clumps of various concentrations. Quillen & Thorndike (2002) have developed a numerical model of type III for the  $\epsilon$  Eridani dust ring using the numerical technique developed by Kuchner & Holman (2001). They find that dust released just outside a planet with eccentricity 0.3 and mass  $\mu = 10^{-4}$  becomes trapped in the 5:3 and the 3:2 MMRs with the planet, and forms a blobby eccentric ring like the one in Figure 1. The second order 5:3 MMR may be relatively strong because the first order resonances suffer from the cancellation described in Section 3.4. Though dust trapped in these resonances probably forms relatively narrow rings, the large beam of the JCMT could easily blur such a narrow blobby ring into something resembling the Holland et al. (1998)

image, as Quillen & Thorndike (2002) illustrate.

**Fomalhaut:** The A3 V star Fomalhaut has a circumstellar dust cloud, recently identified as ring with an azimuthal asymmetry representing  $\sim 5\%$  of the total flux from the disk (Holland et al. 2003). This ring is difficult to classify, since it is roughly  $20^\circ$  from edge-on. Wyatt & Dent (2002) suggest that the dust may be trapped in a 2:1 MMR with a planet, and Holland et al. (2003) suggest that the dust might be trapped in a 1:1 MMR with a planet. However, the 1:1 MMRs are much harder to populate with dust than the MMRs we consider here, and contrary to Ozeroy et al. (2000), we consider it improbable that a single MMR, even the 2:1, could dominate the appearance of a real dust cloud, particularly one as collisional as Fomalhaut's. More likely, the structure in the Fomalhaut ring arises from collisions Wyatt & Dent (2002) or if resonant trapping is responsible for the azimuthal structure, there is another clump to be found, perhaps obscured by the limb-brightening.

We know no observed examples of case II rings. However, the close-in extrasolar planets with periods less than  $\sim 30$  days have nearly circular orbits, probably due to tidal effects (Marcy & Butler 2000). Any dust disks associated with these planets could form examples of case II.

## 5.2. Other Considerations

We have only addressed the geometry of resonant dust orbits. A variety of other phenomena may affect the appearance of an actual debris disk. For example, we have not discussed how the resonances are populated. Different resonances may dominate when a disk is fed by a belt of asteroids or comets whose orbits are restricted to a small region of phase space.

Furthermore, many known dust disks are collisional. For systems like the rings of Saturn, where each particle has a collision roughly once per orbit, the collisions dominate the resonant effects we catalog here, and a fluid description of the particles becomes more appropriate. Collisions which occur on intermediate time scales, however, may leave particles trammelled in the net of the underlying strong resonances, altering only the spectrum of populated MMRs. For example, mutual collisions among dust grains may destroy dust particles before they can access all the strong resonances; this effect would preserve the basic four structures shown in Figure 1.

We have also neglected the terms in MMRs that depend on the inclinations, and restricted our analysis to planets with moderate eccentricity. At high planet inclinations

( $i^2 \sim 1$ ) and eccentricities ( $e^2 \sim 1$ ), many new terms in the disturbing function become relevant. These effects can alter the basic resonant geometries.

Many planetary systems have more than one planet; we have also only considered the effects of one planet. Since we are only interested in high-contrast structures, we may justify this approach by saying we only care about the first massive planet to encounter the inspiraling dust—massive enough to create a high-contrast structure by ejecting most of the dust grains as they pass. For example, in simulations by Liou & Zook (1999), Neptune ejects most of the inspiraling Kuiper belt particles before they can encounter any other planets; we are interested in analogous planets. However, the secular evolution of a multiple-planet system may affect how a planet interacts with a dust cloud, even if little dust reaches most of the planets, and they do not carve their own signatures.

Finally, we have tacitly assumed that the dust cloud is observed face on. Disks which are tilted from face-on may show a variety of asymmetries due to effects other than resonant trapping, such as the IRAS/DIRBE dust bands (Hauser et al. 1984), secular warps (Augereau et al. 2001), and limb brightening.

## 6. CONCLUSIONS

Four basic structures probably represent the range of high-contrast resonant structures a planet with eccentricity  $\lesssim 0.6$  can create in disk of dust released on low-eccentricity orbits: a ring with a gap at the location of the planet, a smooth ring, a blobby eccentric ring, and an offset ring plus a pair of clumps. Some of these structures have slowly become revealed in numerical simulations of particular debris disks; we have chased them to their dens in the resonant landscape of the 3-body problem. The crude key we have assembled should help classify the debris disk structures seen by upcoming telescopes like SIRTF, SOFIA, ALMA, JWST and Darwin/TPF.

Observing one of these structures instantaneously should allow us to categorize the planet as high or low mass (compared to Jupiter orbiting the Sun), and low or moderate eccentricity (compared to  $e_0 \sim 0.2$ ). In the case of a ring with a gap or an offset ring plus a pair of clumps, the image of the face-on cloud directly indicates the current location of the planet and points to its longitude of perihelion. In the case of a blobby eccentric ring, numerical modeling can potentially reveal these parameters.

We thank Tommy Grav, Sean Moran and Mike Lecar for helpful discussions. This work was performed in part under contract with the Jet Propulsion Laboratory (JPL) through the

Michelson Fellowship program funded by NASA as an element of the Planet Finder Program. JPL is managed for NASA by the California Institute of Technology.

## REFERENCES

Augereau, J. C., Nelson, R. P., Lagrange, A. M., Papaloizou, J. C. B., & Mouillet, D. 2001, *A&A*, 370, 447

Banaszkiewicz, M., Fahr, H. J., & Scherer, K. 1994, *Icarus*, 107, 358

Beauge, C. & Ferraz-Mello, S. 1994, *Icarus*, 110, 239

Brouwer, D. & Clemence, G. M. 1961, Methods of Celestial Mechanics (New York: Academic Press)

Burns, J. A., Lamy, P., & Soter, S. 1979, *Icarus*, 40, 1

Burrows, C. J., Krist, J. E., Stapelfeldt, K. R., and the WFPC2 Investigation Definition Team 1995, *BAAS*, 187, 3205

Dermott, S.F., Jayaraman, S., Xu, Y. L., Gustafson, B.Å.S. and Liou, J.-C. 1994, *Nature*, 369, 719

Dermott, S.F., Nicholson, P. D., Burns, J. A., & Houck, J. R. 1985, in Properties and Interactions of Interplanetary Dust, ed. R. H. Giese & P. Lamy (Dordrecht:Reidel), 395

Duncan, M., Quinn, T. & Tremaine, S. 1989, *Icarus*, 82, 402

Fixsen, D. J. & Dwek, E. 2002, *ApJ*, 578, 1009

Gold, T. 1975, *Icarus*, 25, 489

Greaves, J. S., Holland, W. S., Moriarty-Schieven, G., Jenness, T., Dent, W. R. F., Zuckerman, B., McCarthy, C., Webb, R. A., Butner, H. M., Gear, W. K. and Walker, H. J. 1998, *ApJ*, 506, L133.

Greenberg, R. 1978, *Icarus*, 33, 62

Grun, E., Zook, H. A., Fechtig, H. & Giese, R. H. 1985, *Icarus*, 62, 244

Hauser, M. G., Gillett, F. C., Low, F. J., Gautier, T. N., Beichman, C. A., Aumann, H. H., Neugebauer, G., Baud, B., Boggess, N., & Emerson, J. P. 1984, *ApJ*, 278, L15

Holland, W. S., Greaves, J. S., Dent, W. R. F., et al. 2003, *ApJ*, 582, 1141

Holland, W. S., Greaves, J. S.; Zuckerman, B., Webb, R. A., McCarthy, C., Coulson, I. M., Walther, D. M., Dent, W. R. F., Gear, W. K., Robson, I. 1998, *Nature*, 392, 788

Jackson, A. A. and Zook, H. A. 1989, *Nature*, 337, 629

Koerner, D W., Sargent A. I., & Ostroff, N. A., 2001, *ApJ*, 560, L181

Kuchner, M. J., Reach, W. T., & Brown, M. E. 2000, *Icarus*, 145, 44

Kuchner, M. J. and Holman, M. 2001, presented at the December 2001 Division of Planetary Sciences meeting

Lazzaro, D., Sicardy, B., Roques, F. & Greenberg, R. 1994, *Icarus*, 108, 59

Lecavelier Des Etangs, A., Scholl, H., Roques, F., Sicardy, B., & Vidal-Madjar, A. 1996, *Icarus*, 123, 168

Liou, J.-C. and Zook, H. A. 1997, *Icarus*, 128, 354

Liou, J.-C. and Zook, H. A. 1999, *AJ*, 118, 580

Marcy, G. W. & Butler, R. P. 2000, *PASP*, 768, 137

Marzari, F. & Vanzani, V. 1994, *A&A*, 283, 275

Murray, C. D. & Dermott, S. F. 1999, *Solar System Dynamics* (New York: Cambridge Univ. Press)

Ozernoy, L. M., Gorkavyi, N. N., Mather, J. C., & Taidakova, T. A. 2000, *ApJ*, 537, L147

Quillen, A. C. & Thorndike, S. 2002, *ApJ*, 578, L149

Reach, W. T. 1991, *ApJ*, 369, 529

Reach, W. T., Franz, B. A., Weiland, J. L., Hauser, M. G., Kelsall, T. N., Wright, E. L., Rawley, G., Stemwedel, S. W. and Spiesman, W. J. 1995, *Nature*, 374, 521

Robertson, H. P. 1937, *MNRAS*, 97, 423

Roques, F., Scholl, H., Sicardy, B., Smith, B. A. 1994, *Icarus*, 108, 37

Schneider, G., Smith, B. A., Becklin, E. E., Koerner, D. W., Meier, R., Hines, D. C., Lowrance, P. J., Terrile, R. J., Thompson, R. I., & Rieke, M. 1999, *ApJ*, 513, L127

Sicardy, B., Beauge, C., Ferraz-Mello, S., Lazzaro, D., & Roques, F. 1993, *CeMDA*, 57, 373

Weidenschilling, S. J. & Jackson, A. A. 1993, *Icarus*, 104, 244

Wisdom, J. 1980, *AJ*, 85, 1122

Wisdom, J. 1983, *Icarus*, 56, 51

Wilner, D. J., Holman, M. J., Kuchner, M. J., & Ho, P. T. P. 2002, *ApJ*, 569, L115

Wyatt, M. C. & Dent, W. R. F. 2002, *MNRAS*, 334, 589

Wyatt, M. C., Dermott, S. F., Telesco, C. M., Fisher, R. S., Grogan, K., Holmes, E. K., & Piña, R. K. 1999, *ApJ*, 527, 918

Wyatt, S. P. & Whipple, F. L. 1950, *ApJ*, 111, 134

Table 1: Resonant Arguments.

Resonance	Nominal $1/\alpha$	$e_{forced}/e_0$	Argument	Leading Term in $F(\alpha, e, e_0)$
6:5	1.13	0.96	$6\lambda - 5\lambda_0 - \varpi_0$	$-4.44181 e_0$
			$6\lambda - 5\lambda_0 - \varpi$	$4.87053 e$
5:4	1.16	0.94	$5\lambda - 4\lambda_0 - \varpi_0$	$-3.64001 e_0$
			$5\lambda - 4\lambda_0 - \varpi$	$4.07424 e$
4:3	1.21	0.92	$4\lambda - 3\lambda_0 - \varpi_0$	$-2.83462 e_0$
			$4\lambda - 3\lambda_0 - \varpi$	$3.27756 e$
3:2	1.31	0.87	$3\lambda - 2\lambda_0 - \varpi_0$	$-2.02226 e_0$
			$3\lambda - 2\lambda_0 - \varpi$	$2.48115 e$
2:1	1.59	0.74	$2\lambda - \lambda_0 - \varpi_0$	$-1.18945 e_0$
			$2\lambda - \lambda_0 - \varpi^a$	$0.426628 e$
3:1	2.08	0.58	$3\lambda - \lambda_0 - 2\varpi_0$	$0.598757 e_0^2$
			$3\lambda - \lambda_0 - \varpi_0 - \varpi$	$-2.21298 e_0 e$
			$3\lambda - \lambda_0 - 2\varpi^a$	$-0.514804 e^2$
4:1	2.52	0.49	$4\lambda - \lambda_0 - 3\varpi_0$	$-0.244422 e_0^3$
			$4\lambda - \lambda_0 - 2\varpi_0 - \varpi$	$1.61636 e_0^2 e$
			$4\lambda - \lambda_0 - \varpi_0 - 2\varpi$	$-3.51697 e_0 e^2$
			$4\lambda - \lambda_0 - 3\varpi^a$	$1.32796 e^3$
5:1	2.92	0.42	$5\lambda - \lambda_0 - 4\varpi_0$	$0.0848968 e_0^4$
			$5\lambda - \lambda_0 - 3\varpi_0 - \varpi$	$-0.855830 e_0^3 e$
			$5\lambda - \lambda_0 - 2\varpi_0 - 2\varpi$	$3.20820 e_0^2 e^2$
			$5\lambda - \lambda_0 - \varpi_0 - 3\varpi$	$-5.28443 e_0 e^3$
			$5\lambda - \lambda_0 - 4\varpi^a$	$2.24457 e^4$

<sup>a</sup>Includes contribution from indirect term.